

Current-Corrected Cycling Strategies for True Electrode Performance Measurement

Zilai Yan,^[b] Benjamin Scott,^[b] Stephen L. Glazier,^[c] and Mark N. Obrovac^{*[a]}

In battery research, galvanostatic cycling is the most widely used strategy to evaluate electrode performance. By applying pre-set current throughout the test, this method often fails to accurately reflect electrode performance at the designed cycling rate (particularly for high-rate cycling) because the actual capacity can be considerably affected by polarization and electrode degradation. To address this issue, a current-corrected cycling method is proposed, in which the current is actively

adjusted during cycling based on the measured capacity of previous cycles. Compared to the traditional method, which may result in cycling rates that are hundreds of times faster than the designed rate, the proposed cycling strategy can effectively measure rate-dependent electrode performance precisely at designated rates. The authors believe this method is highly useful in electrode/battery performance evaluation for practical cell design, particularly in fast-charging applications.

1. Introduction

Rechargeable batteries have been identified as a key technology, enabling electric vehicles and emerging as a strong candidate for grid energy storage.^[1-3] To improve battery performance, extensive research in new electrodes has taken place via their synthesis, and evaluation for their electrochemical performance.^[4-7] One of the most common strategies to investigate electrode performance is the utilization of galvanostatic cycling.^[8-10] In each charge/discharge step, a constant current is applied until a designed potential is reached. The C-rate is widely used to describe the discharge/charge rate and is defined as the current at which a cell can be fully charged or discharged in one hour. A cell's cycling rate is commonly expressed in terms of the C-rate as C/#, where # is the number of hours desired to reach the end of discharge or charge.^[11] This key parameter is often presented along with measured capacity since cell/electrode electrochemical behavior is a strong function of the cycling rate.

For traditional galvanostatic cycling (TGC), the current value is generally set according to the predicted cell/electrode capacity and remains unchanged throughout the test. To test electrode performance under different rates (e.g., in a rate cycling test), a universal current value (in most cases obtained from the theoretical capacity at low rates) is unfortunately

used, due to the difficulty in predicting the capacity under these rates.^[13,14] In reality, high-rate performance is likely measured at a much higher rate than the designed rate because of significantly declined cell capacity due to polarization/diffusion effects. Available data at designed cycling rates is challenging to gather, seriously hindering high-rate battery development.^[12] In addition, electrodes suffer degradation and capacity loss. This also results in accelerated actual cycling rates,^[15] as illustrated in Figure S1. Thus, the observed performance of a degraded electrode during TGC at high rates has little to do with its ability to operate under a fixed discharge/charge time.

Herein, a current-corrected galvanostatic cycling (CCGC) strategy is proposed, to ensure that electrodes and related electrochemical cells of interest are evaluated at designed cycling rates, while the TGC results are presented as a comparison.

2. Results and Discussion

CCGC can be accomplished by setting the current of each cycle based on the capacity of previous cycle(s), except the initial cycle which was determined from the theoretical capacity. During each charge/discharge process, the current is set to be constant, as in traditional galvanostatic cycling.

Figure 1(a) shows the capacity vs. cycle number of graphite electrodes cycled under CCGC and TGC conditions. When graphite electrodes were cycled at a slow C/20 rate, the graphite capacity remained constant and is nearly identical for both cycling methods, even after 250 cycles. This result indicates that the graphite electrodes remained highly reversible throughout this test. Differences in capacities become apparent for electrodes cycled at a C/3 rate. For each 50-cycle loop, graphite electrodes cycled under TGC conditions showed rapid initial capacity fade during the first 10 cycles and then slightly recovered their capacity (the reasons for this behavior are explained below). Correspondingly, during TGC the actual

[a] Prof. M. N. Obrovac
Department of Chemistry
Department of Physics and Atmospheric Science
Dalhousie University
Halifax, NS, B3H 4R2, Canada
E-mail: mnobrovac@dal.ca

[b] Z. Yan, B. Scott
Department of Chemistry
Dalhousie University
Halifax, NS, B3H 4R2, Canada

[c] Dr. S. L. Glazier
Novonix Battery Testing Services Ltd.
Bedford, NS, Canada

 Supporting information for this article is available on the WWW under
<https://doi.org/10.1002/batt.202100345>

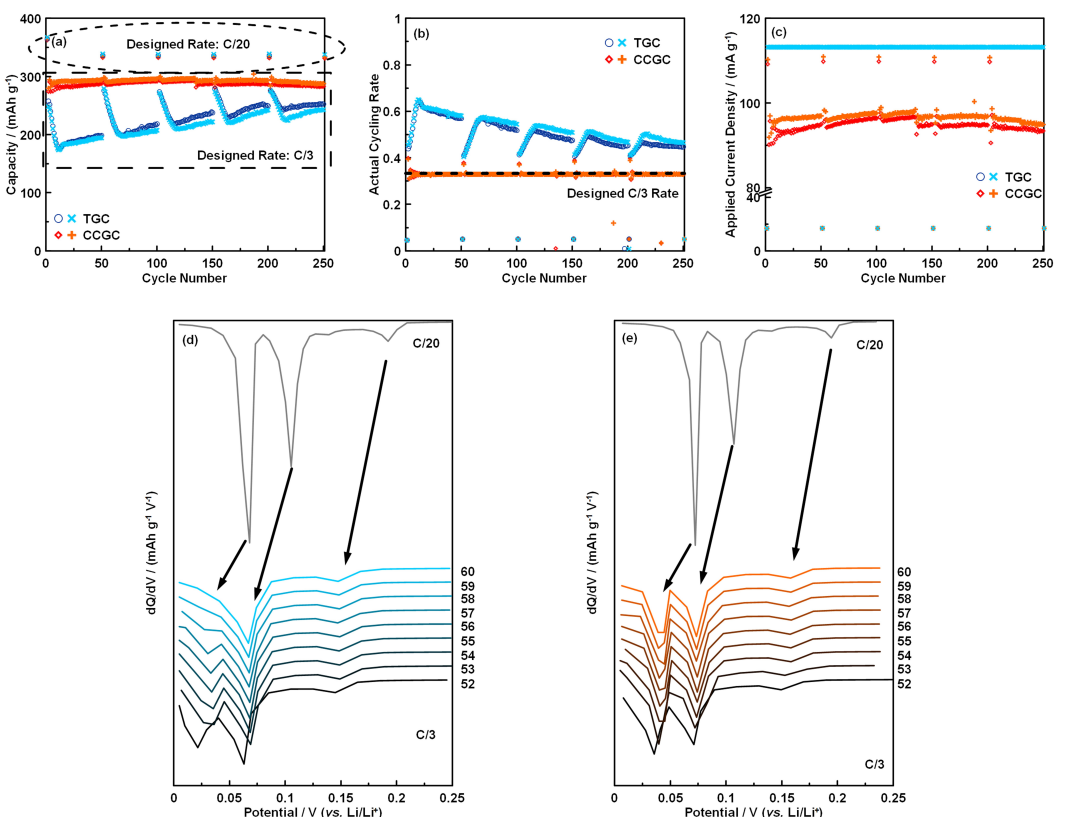


Figure 1. a) Lithiation capacity, b) the actual cycling rate, and c) the applied current density of graphite electrodes in half cells cycled with CCGC and TGC protocols. In each 50 cycles, the graphite electrodes were first cycled at the rate of C/20, followed by 49 cycles at the rate of C/3 between 5 mV and 0.9 V. The dQ/dV curves of the graphite electrodes at indicated cycle number, cycled with d) TGC and e) CCGC protocols. Arrows indicate how the differential capacity peaks of graphite are shifted between C/20 and C/3 cycling rates.

cycling rate increased during the initial capacity fade of each 50-cycle loop to almost as twice the designed rate (as shown in Figure 1b) since the applied current density during the TGC test remained unchanged, as shown in Figure 1(c). In contrast, the applied current density at each cycle was actively modified in the CCGC method. For example, as shown in Figure 1(c), during CCGC a relatively high current density ($\sim 110 \text{ mA g}^{-1}$) was applied during the initial C/3 cycle in each 50-cycle loop, since this rate was based on the previous cycle's capacity, which was conducted at a lower C/20 rate and consequently had a high reversible capacity of $\sim 330 \text{ mAh g}^{-1}$. According to the CCGC protocol, the current density was quickly modified to $\sim 96 \text{ mA g}^{-1}$, due to the relatively smaller reversible capacity measured at the C/3 cycling rate. As a result, the graphite capacity remained stable at $\sim 290 \text{ mAh g}^{-1}$ during CCGC cycling (Figure 1a) and the actual cycling rates were well controlled, staying at the designed C/3 rate (Figure 1b).

Moreover, as shown in Figure 1(c), despite the continual adjustments in current, the applied current density remained relatively stable at about $90\text{--}95 \text{ mA g}^{-1}$ during C/3 cycling. Nevertheless, the CCGC method could be improved further if the simple method of averaging the capacities of previous cycles to determine the cycling rate of the next cycle was modified, e.g., by utilizing the gradient descent method, (which could not be accommodated with the utilized charger's

software) or at least by only including those previous cycles measured at the same rate in the averaging.

Figure 1(d and e) shows differential capacity curves of graphite cycled under C/3 TGC and CCGC conditions, respectively, during cycles 52–60. This cycling range corresponds to the region of severe fade in the TGC cycled cell during the first 10 cycles of the second 50-cycle loop. Also shown in each figure is the differential capacity curve of graphite cycled at C/20 rate for reference. Graphite has three major dQ/dV peaks at ~ 0.2 , ~ 0.1 , and $\sim 0.07 \text{ V}$ during slow lithiation, corresponding to the formation of LiC_{24} , LiC_{12} , and LiC_6 , respectively.^[16] During fast charging (at the C/3 rate), the dQ/dV curves become broader and are shifted towards low potentials for both the TGC and CCGC methods, as shown in Figure 1(d and e). The peaks corresponding to LiC_6 formation shift from $\sim 0.07 \text{ V}$ at C/20 to $\sim 0.03 \text{ V}$ at C/3. This peak is heavily affected by the induced polarization using TGC, resulting in capacity loss and poor cycling performance. A slight recovery in the capacity after the initial 10 cycles is also related to a partially improved kinetics during LiC_6 formation. Figure S2 shows dQ/dV curves of the graphite electrode between cycles 60–100 for the TGC method. The LiC_6 formation peak appears after cycle 65 lithiation endpoint. The intensity of this peak keeps growing during these cycles. In contrast, since the cell cycled utilizing CCGC is charged and discharged at a lower and more constant rate, its differential capacity peaks are sharper and show less

variability between cycles. In addition, the narrower LiC₆ formation peak does not become truncated by the lower cutoff potential and retains its capacity.

As shown in Figure S3, graphite electrodes at a C/20 rate have a similar overpotential (considered as the sum of inherent zero-current potential hysteresis and cell-resistance induced polarization^[17]) of ~0.04 V under these two cycling methods. At a C/3 rate, CCGC results have an average overpotential of ~0.085 V at initial cycles, that gradually increases up to ~0.12 V after 250 cycles. At the same rate, TGC results have a higher overpotential of 0.02–0.03 V during cycling.

Graphite electrodes were cycled at different rates ranging from C/20 to 5C using TGC and CCGC methods (Figure 2). For TGC, the capacity decreases quickly at rates higher than C/5 and becomes negligible when the rate is \geq 2C. This is because the actual cycling rates are much higher than the designed rates when the capacity becomes lower due to polarization, as shown in Figure 2(b). For instance, at a designed 5C rate, the observed actual cycling rate for TGC is 1200C–3600C, about 500 times higher. In addition to the low capacities at high rates, at C/2 the capacity is not stable, due to the increasing overpotential, which causes staging plateaus to be truncated by the lower potential cutoff.

In contrast, the actual cycling rates are well managed with the CCGC method. Since the cycling current is based on the average cell capacity of the previous four cycles, the first cycle of each rate step has a low capacity (Figure 2a) and an actual cycling rate that is higher than the designed rate (Figure 2b). As shown in Figure 2(b), as cycling proceeds, the current then corrects itself so that the actual current approaches the designed current after a few cycles. For subsequent cycles, there are small oscillations in the actual rate around the designed rate. This is due to an overcorrection of the cell current, as shown in Figure S4 for cycling at the rate of 5C. Again, some common optimization methods, such as gradient descent, should be adapted in future work as an efficient strategy for this current adjustment. Nevertheless, for the simple averaging method used here, the oscillations become small as cycling proceeds at the same rate. Here, the level of accuracy from these small oscillations ($\pm < 10.6\%$ of the

designed rate during the last five cycles) was deemed acceptable.

The differences between the TGC and CCGC results in Figure 2(b) are remarkable. Even at 5C cycling, the graphite electrode still can deliver a capacity of $\sim 50 \text{ mAh g}^{-1}$ utilizing CCGC. Moreover, the impact of increasing polarization on capacity is significantly reduced for CCGC, so that there is no observable capacity fade in each rate step (contrasted to the rapid fade of the same electrode at C/2 for TGC cycling). We believe that the CCGC rate test results shown in Figure 2(a) provide significant additional information to the TGC results and even may be superior for gaining practical knowledge about materials rate performance. For instance, if a device requires a cell to charge and discharge in 2 hours, it can be easily seen from the CCGC results that, when designing such a cell, graphite should be assumed to have a capacity of about 250 mAh g^{-1} . In contrast, the TGC results provide no useful information on how such a cell should be designed. The CCGC method can provide much needed information on electrode performance, especially at high rates, which we believe will be beneficial for researchers in designing high-rate batteries.

The use of CCGC as a method to investigate the degradation of electrode materials was also explored. Here materials degradation refers to processes that cause the loss of active lithium and/or the loss of sites available for lithium insertion, resulting in capacity fade. Most often, degradation processes are accompanied by an increase in electrode impedance, either as true hysteresis or increased polarization, which can also cause capacity fade. When TGC is used, the actual cycling rate increases as material degradation occurs, further increasing polarization, and further inducing capacity fade. This makes it difficult to understand how much capacity fade is coming from increased impedance/increased actual cycling rate and how much fade is attributable to materials degradation.

LiNiO_2 is well known to suffer from capacity fade due to cation mixing and structural degradation associated with the oxidation of Ni^{2+} in Li^+ sites during delithiation.^[15,18] This causes both increased impedance and trapped Li^+ and empty Li^+ sites that are inaccessible towards lithiation. Under the CCGC and TGC methods, the LiNiO_2 electrodes have almost the same

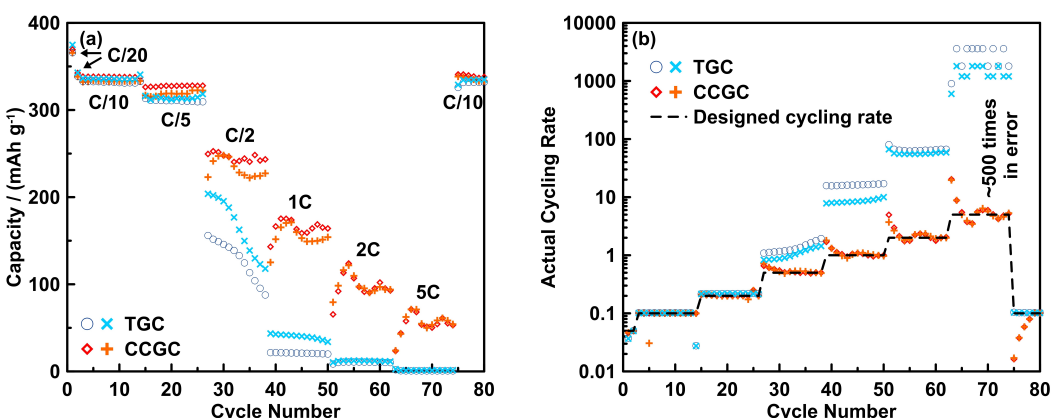


Figure 2. a) Lithiation capacity and b) the actual cycling rate of graphite electrodes cycled at different rates using CCGC and TGC.

capacity fade behavior during the first 70 cycles, as shown in Figure 3. During this time, overpotential in both cells increases in the same manner, as shown in Figure 3(b). CCGC cycling has no impact on this increased polarization, which may indicate a true electrode performance. The increased polarization results in the 4.2 V delithiation differential capacity peak becoming truncated by the upper cutoff potential, resulting in the observed capacity fade. Differences between the TGC and CCGC methods become observable after 70 cycles, where the capacity retention of CCGC cycled LiNiO_2 becomes higher than LiNiO_2 cycled utilizing TGC. After 300 cycles, the capacity retentions of LiNiO_2 electrodes evaluated by CCGC and TGC are $\sim 56\%$ and $\sim 45\%$, respectively (Figure 3(a), bottom panel). As shown in Figure 3(b) after cycle 70, cell polarization increases much faster under TGC than that under CCGC. This result indicates that the TGC can induce additional polarization during electrode degradation, resulting in excessive capacity fade. This effect is reduced in CCGC cycling, which is less susceptible to polarization induced capacity fade.

In addition to these results, we have also found that the CCGC method applied to Si-anodes (Figures S6–S8) and practical full cells (Figure S9) can improve consistency in voltage behavior and result in cell fade rates that better reflect true degradation behavior. The current-correction strategy in

this work replies on previous cycle performance. The CCGC method could be broadly adapted by other optimization algorithm and capacity estimation approaches (such as impedance-based methods^[19]), particularly for realistic applications where batteries are rarely cycled at a full range of charge and discharge.

3. Conclusions

In summary, an advanced galvanostatic cycling method, termed current-corrected galvanostatic cycling (CCGC), has been developed to evaluate the electrode performance under designed cycling rates. With traditional galvanostatic cycling (TGC), actual cycling rates can deviate significantly from the designed cycling rate. For instance, it was observed here that when using TGC to cycle graphite electrodes at a designed 5C rate, the actual cycling rate was ~ 500 times larger. As a result, TGC cycling is a poor indication of a cell's ability to cycle at a designed rate. Furthermore, under such conditions, positive feedback exists where capacity fade results in increased actual rate, leading to increased overpotential and further capacity fade. This makes fade from cell degradation very difficult or

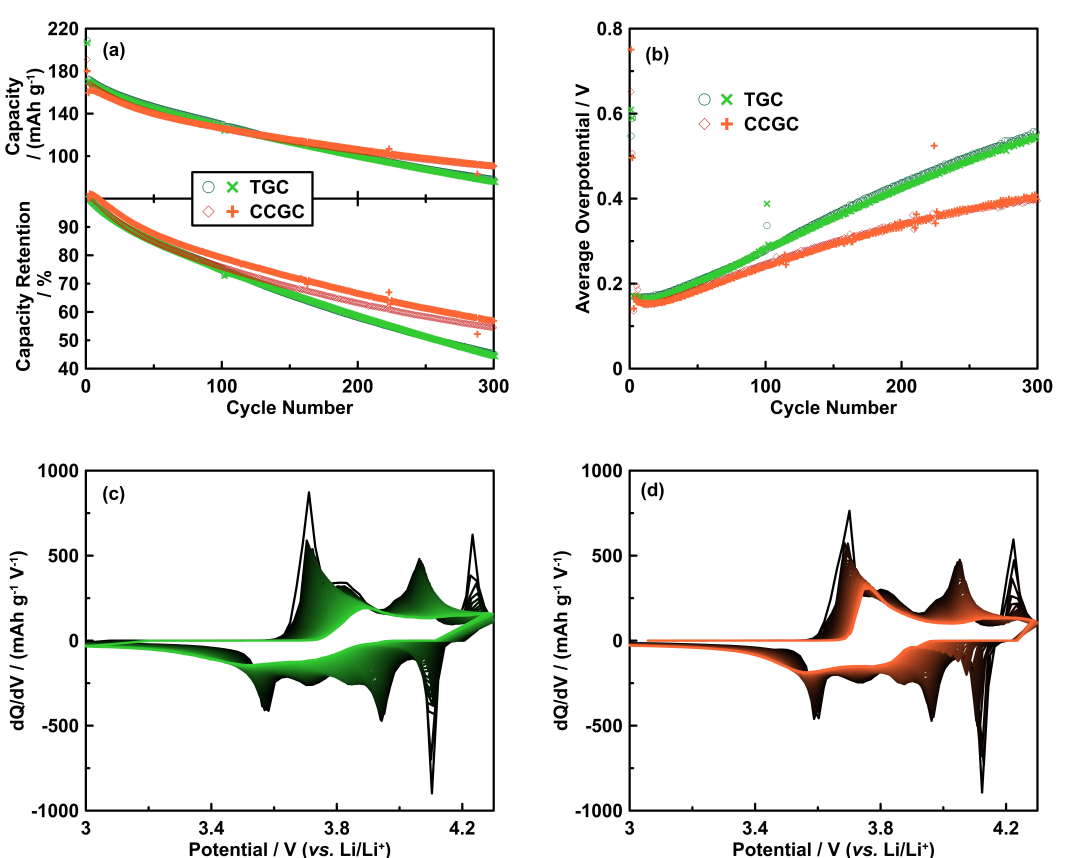


Figure 3. a) Delithiation capacity (top panel) and capacity retention (bottom panel) of LiNiO_2 electrodes cycled on the basis of TGC and CCGC. The initial cycle was set at the rate of C/20, followed by the cycling at C/2 rate. The actual cycling rate for LiNiO_2 electrodes under TGC at the second delithiation is C/1.4. b) Average overpotential of the LiNiO_2 electrodes cycled by TGC and CCGC. The dQ/dV curves between 2th and 300th cycle of the LiNiO_2 electrodes c) TGC and d) CCGC. Later cycles are towards either green or orange.

impossible to deconvolute from accelerating increases in overpotential induced by the TGC method.

In contrast, it was found that the use of CCGC can totally avoid such errors, providing the electrode performance exactly under designed cycling rates. On the basis of this new cycling strategy, the electrode electrochemical properties without induced polarization can be obtained, as exemplified with LiNiO₂ and Si electrodes. The authors believe this method is highly useful in electrode/battery performance evaluation for practical cell design and may have application in improving cycle life of practical cells, particularly in fast-charging applications.

Experimental Section

Electrochemical cell preparation

Coin cell construction was conducted in an Ar-filled glovebox using standard 2325 coin cell hardware. For cells with graphite or Si electrodes, 1 M LiPF₆ in ethylene carbonate (EC):diethyl carbonate (DEC):fluoroethylene carbonate (FEC) (3:6:1 v/v/v, all battery grade from BASF) was used as electrolyte. For cells with LiNiO₂ electrodes, 1 M LiPF₆ in EC:DEC (1:2 v/v) was used as electrolyte. Two layers of Celgard-2300 separator and one layer of polyethylene blown microfiber nonwoven fabric (BMF) (3 M Company) were used as cell separators. Each electrode was paired with a 2.57 cm² circular lithium metal (thickness of 0.38 mm, 99.9%, Sigma-Aldrich) electrode. 402040-size pouch-type Li-ion cells (capacity of ~275 mAh) used in this study used an artificial graphite negative electrode with a 12.4 mg cm⁻² loading mass, and a NMC622 positive electrode with a 19.4 mg cm⁻² loading mass. After vacuum drying overnight, 1.2 g of electrolyte (1.2 M LiPF₆ in EC:ethyl methyl carbonate (EMC):dimethyl carbonate (DMC) 25:5:70 by weight with 2 wt.% vinylene carbonate (VC)) was added into the dry pouch cells in a dry room with an operating dew point of -50°C, then vacuum sealed. Formation cycles were conducted by holding cells at 1.5 V for 24 hours at 40°C, then charging to 4.2 V at a rate of C/20, and then discharge to 3.8 V at C/20 rate.

Electrochemical testing

Cells were evaluated using a MacCor Series 4000 Automated Test System and thermostatically controlled at 30.0±0.1°C, unless otherwise specified. Pouch cells were cycled between 2.8–4.2 V. In most cases, CCGC can be accomplished by setting the current of each cycle based on the capacity of the previous cycle, except the initial cycle which was determined from the theoretical capacity. However, it was found that this method failed to achieve convergent cycling results in the cases where the cycling capacity was highly sensitive to the current density (e.g., graphite electrodes cycled at high rates (>1 C) during the rate cycling in this work). Therefore, this was resolved by setting the current according to the average capacity from the previous four cycles (starting from the 5th cycle) for cycling rate testing. In this case, the initial-cycle current was also determined from the theoretical capacity. From the second to the fourth cycle, the current was determined by the average capacity of previous cycles. Ideally, common optimization algorithms, such as gradient descent, should be used if enabled by the charger's software.

Acknowledgements

The authors acknowledge financial support from NSERC, NOVONIX Battery Technology Solutions Ltd., the Canada Foundation for Innovation, and the Atlantic Innovation Fund for this work.

Conflict of Interest

The authors declare no conflict of interest.

Data Availability Statement

Research data are not shared.

Keywords: batteries • electrochemistry • energy conversion• fast charging • polarization

- [1] S. Chu, A. Majumdar, *Nature* **2012**, *488*, 294–303.
- [2] Z. Yang, J. Zhang, M. C. W. Kintner-Meyer, X. Lu, D. Choi, J. P. Lemmon, J. Liu, *Chem. Rev.* **2011**, *111*, 3577–3613.
- [3] H.-H. Ryu, H. H. Sun, S.-T. Myung, C. S. Yoon, Y.-K. Sun, *Energy Environ. Sci.* **2021**, *14*, 844–852.
- [4] M. Ue, K. Sakaushi, K. Uosaki, *Mater. Horiz.* **2020**, *7*, 1937–1954.
- [5] J. B. Goodenough, *J. Solid State Electrochem.* **2012**, *16*, 2019–2029.
- [6] J. Huang, P. Zhong, Y. Ha, D.-H. Kwon, M. J. Crafton, Y. Tian, M. Balasubramanian, B. D. McCloskey, W. Yang, G. Ceder, *Nat. Energy* **2021**, *6*, 706–714.
- [7] Z.-J. Han, N. Yabuuchi, K. Shimomura, M. Murase, H. Yui, S. Komaba, *Energy Environ. Sci.* **2012**, *5*, 9014–9020.
- [8] J. Xiao, Q. Li, Y. Bi, M. Cai, B. Dunn, T. Glossmann, J. Liu, T. Osaka, R. Sugiura, B. Wu, J. Yang, J.-G. Zhang, M. S. Whittingham, *Nat. Energy* **2020**, *5*, 561–568.
- [9] Y. Son, T. Lee, B. Wen, J. Ma, C. Jo, Y.-G. Cho, A. Boies, J. Cho, M. De Volder, *Energy Environ. Sci.* **2020**, *13*, 3723–3731.
- [10] A. J. Merryweather, C. Schnedermann, Q. Jacquet, C. P. Grey, A. Rao, *Nature* **2021**, *594*, 522–528.
- [11] C. Heubner, M. Schneider, A. Michaelis, *Adv. Energy Mater.* **2020**, *10*, 1902523.
- [12] X.-G. Yang, T. Liu, Y. Gao, S. Ge, Y. Leng, D. Wang, C.-Y. Wang, *Joule* **2019**, *3*, 3002–3019.
- [13] A. S. Hameed, A. Katogi, K. Kubota, S. Komaba, *Adv. Energy Mater.* **2019**, *9*, 1902528.
- [14] Y. Cao, T. D. Hatchard, R. A. Dunlap, M. N. Obrovac, *J. Mater. Chem. A* **2019**, *7*, 8335–8343.
- [15] H. Li, N. Zhang, J. Li, J. R. Dahn, *J. Electrochem. Soc.* **2018**, *165*, A2985–A2993.
- [16] Q. Liu, S. Li, S. Wang, X. Zhang, S. Zhou, Y. Bai, J. Zheng, X. Lu, *J. Phys. Chem. Lett.* **2018**, *9*, 5567–5573.
- [17] S. L. Glazier, K. J. Nelson, J. P. Allen, J. Li, J. R. Dahn, *J. Electrochem. Soc.* **2017**, *164*, A1203–A1212.
- [18] H.-H. Ryu, G.-T. Park, C. S. Yoon, Y.-K. Sun, *J. Mater. Chem. A* **2019**, *7*, 18580–18588.
- [19] M.-H. Hung, C.-H. Lin, L.-C. Lee, C.-M. Wang, *J. Power Sources* **2014**, *268*, 861–873.

Manuscript received: November 15, 2021
Version of record online: December 1, 2021